



CDF note 8827

Measurement of the Inclusive Jet Cross Section in $Z(\rightarrow ee) + \text{jets}$ Production

The CDF Collaboration

URL <http://www-cdf.fnal.gov>

(Dated: May 23, 2007)

We report on preliminary measurements of inclusive $Z(\rightarrow ee) + \text{jets}$ production cross sections as a function of the jet transverse momentum and jet multiplicity in $p\bar{p}$ collisions at $\sqrt{s} = 1.96$ TeV using data collected with the upgraded Collider Detector at Fermilab in Run II, corresponding to an integrated luminosity of 1.1 fb^{-1} . The measurement is carried out for jets with rapidity $|y^{\text{jet}}| < 2.1$ and transverse momentum in the range $p_T^{\text{jet}} > 30 \text{ GeV}/c$. Next-to-leading order perturbative QCD predictions are in good agreement with the measured cross sections.

I. INTRODUCTION

The measurement of inclusive Z +jets production cross sections in $p\bar{p}$ collisions at $\sqrt{s} = 1.96$ TeV provides a stringent test of perturbative Quantum Chromodynamics (pQCD) [1] and is a crucial part of the physics program at the Tevatron since Z +jets processes constitute important backgrounds in searches for new physics like, for example, supersymmetry. Previous results [2] at the Tevatron indicate that the data can be described by leading-order (LO) plus parton shower Monte Carlo predictions. This letter reports on new preliminary measurements on $Z(\rightarrow ee)$ +jets production using 1.1 fb^{-1} of data collected by the CDF experiment in Run II. The measured cross sections are corrected back to the hadron level [3] and compared to next-to-leading order (NLO) pQCD predictions including non-perturbative contributions.

II. MONTE CARLO SIMULATION

Monte Carlo event samples are used to determine the response of the detector and the correction factors to the hadron level. The generated samples are passed through a full CDF detector simulation (based on GEANT3 [4] where the GFLASH [5] package is used to simulate the energy deposition in the calorimeters) and then reconstructed and analyzed using the same analysis chain as for the data. Samples of simulated inclusive $Z(\rightarrow ee)$ +jets events have been generated using the PYTHIA 6.203 [6] Monte Carlo generator. CTEQ5L [7] parton distribution functions (PDFs) are used for the proton and antiproton. The PYTHIA samples have been created using two special tuned sets of parameters, denoted as PYTHIA-TUNE A [8] and PYTHIA-TUNE DW [9], that include enhanced contributions from initial-state gluon radiation and secondary parton interactions between proton/antiproton beam remnants and provide a proper description of the measured jet shapes and energy flows in $Z(\rightarrow ee)$ +jets final states (see Fig. 1). Monte Carlo samples for $t\bar{t}$, $Z(\rightarrow ee) + \gamma$, dibosons and $Z(\rightarrow \tau\tau)$ +jets background processes are generated using PYTHIA-TUNE A.

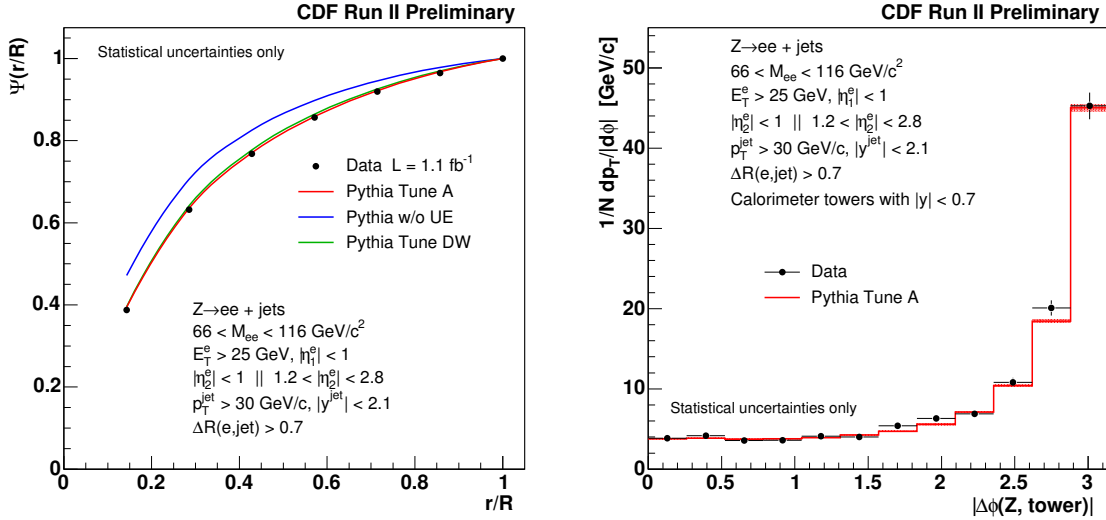


FIG. 1: (left) Measured integrated jet shape compared to different Monte Carlo predictions with different underlying event settings. The measurement only includes statistical uncertainties. (right) Measured energy flow in the transverse plane for Z +jets events. Event-by-event, $\phi = 0$ is defined along the direction of the Z boson. The measurement is performed considering calorimeter towers with $|y| < 0.7$ and compared to PYTHIA TUNE A Monte Carlo prediction. The measurements only include statistical uncertainties.

III. JET RECONSTRUCTION

Jets are reconstructed in data and Monte Carlo simulated events from the energy deposits in the calorimeter towers with transverse momentum above $0.1 \text{ GeV}/c$, using the Midpoint algorithm [10] with cone radius $R=0.7$ and starting from seed towers with transverse momentum above $1 \text{ GeV}/c$. All the towers associated with the reconstructed

electrons [11] in the final state are excluded. The jet transverse momentum, rapidity and azimuthal angle are denoted as $p_{T,\text{cal}}^{\text{jet}}$, $y_{\text{cal}}^{\text{jet}}$, and $\phi_{\text{cal}}^{\text{jet}}$, respectively. The same algorithm is applied to the final state particles [3] in the Monte Carlo generated events, excluding Z decay products, to define jets at the hadron level. The direction of the jets, $y_{\text{cal}}^{\text{jet}}$ and $\phi_{\text{cal}}^{\text{jet}}$, are well reconstructed in the calorimeter with a resolution better than 0.05 units in y and ϕ . The measured $p_{T,\text{cal}}^{\text{jet}}$ systematically underestimates that of the hadron-level jet mainly due to the non-compensating nature of the calorimeter [12], and includes contributions from multiple $p\bar{p}$ interactions per crossing at high instantaneous luminosity. An average correction is applied to the measured $p_{T,\text{cal}}^{\text{jet}}$ to account for those effects [13].

IV. EVENT SELECTION

The measurements presented in this letter correspond to a total integrated luminosity of 1.1 fb^{-1} . Events are collected online using a three-level trigger system. At the first-level trigger, events are required to have a central electromagnetic calorimeter cluster ($|\eta| < 1$) with transverse energy, E_T , above 8 GeV and a track pointing to it with transverse momentum, p_T^{track} , above 8 GeV/c. Similarly, at the second-level (third-level) trigger a central electromagnetic cluster with $E_T > 16$ GeV ($E_T > 18$ GeV) and an associated track with $p_T^{\text{track}} > 8$ GeV/c ($p_T^{\text{track}} > 9$ GeV/c) is required. The events are then required to have two electrons with $E_T^e > 25$ GeV and a reconstructed invariant mass in the range $66 < M_{ee} < 116$ GeV/ c^2 , where the electron candidates are reconstructed using the standard CDF criteria [14] with no isolation requirement applied. In this study, one electron is required to be central ($|\eta^e| < 1$) and fulfill tight selection cuts, while the second electron is required to pass a looser selection and to be either central or forward with $1.2 < |\eta^e| < 2.8$. Finally, the events are selected to have a reconstructed primary vertex with z -position within 60 cm around the nominal interaction point, and at least one jet with $p_{T,\text{cal}}^{\text{jet}} > 30$ GeV/c, rapidity in the range $|y_{\text{cal}}^{\text{jet}}| < 2.1$, and $\Delta R_{e-\text{jet}} > 0.7$, where $\Delta R_{e-\text{jet}}$ denotes the distance ($\eta - \phi$ space) between the jet and each of the two electrons in the final state.

V. BACKGROUND ESTIMATION

The $Z(\rightarrow ee)$ +jets data sample contains background mainly from QCD-jets and W +jets processes that is extracted from data. First, an inclusive jet data sample, with a negligible content on prompt electrons, is employed to estimate the probability, f_e^{jet} , for a jet to pass a given electron selection. Second, a sample of events in data with exactly one reconstructed central-tight electron is selected. For each jet in the event, the electron-jet invariant mass is computed, where the difference between $p_{T,\text{cal}}^{\text{jet}}$ and E_T^e of the corresponding misidentified electron is properly taken into account. Event-by-event, all electron-jet combinations with an invariant mass within $66 < M_{e-\text{jet}} < 116$ GeV/ c^2 are considered in the background calculation, where each combination is weighted by the corresponding f_e^{jet} value, divided by the number of accepted e-jet combinations in the event. The total QCD-jets and W +jets background is then computed in each measured distribution. Other background contributions from $t\bar{t}$, $Z(\rightarrow ee) + \gamma$, dibosons and $Z(\rightarrow \tau\tau)$ +jets final states are estimated using Monte Carlo samples. The total background in inclusive $Z(\rightarrow ee) + \geq N_{\text{jet}}$ production varies between 10 % and 14 % as N_{jet} increases. Good agreement is observed between the data and the $Z(\rightarrow ee) + \geq N_{\text{jet}}$ Monte Carlo plus background prediction in the signal region and in ± 20 GeV/ c^2 sidebands around the selected M_{ee} range, where the background contributions become dominant.

VI. UNFOLDING AND SYSTEMATIC UNCERTAINTIES

The measurements are unfolded back to the hadron level using PYTHIA-TUNE A event samples. The measurements refer to hadron level jets with $p_T^{\text{jet}} > 30$ GeV/c and $|y^{\text{jet}}| < 2.1$, in a well-defined kinematic range for the Z decay products: $E_T^e > 25$ GeV, $|\eta^{e1}| < 1.0$, $|\eta^{e2}| < 1.0$ or $1.2 < |\eta^{e2}| < 2.8$, $66 < M_{ee} < 116$ GeV/ c^2 , and $\Delta R_{e-\text{jet}} > 0.7$. The measurements are corrected for acceptance and smearing effects using a bin-by-bin unfolding procedure, which also accounts for the efficiency of the $Z(\rightarrow ee)$ selection criteria. In order to avoid any potential bias in the unfolding factors, PYTHIA-TUNE A is re-weighted until it accurately follows the measured $p_{T,\text{cal}}^{\text{jet}}$ distributions. The unfolding factors are computed separately for the different inclusive $Z(\rightarrow ee) + \geq N_{\text{jet}}$ final states and vary between 2.0 at low p_T^{jet} and 2.3 at high p_T^{jet} .

A first study of the different systematic uncertainties was carried out [15]. Remaining uncertainties on the Monte Carlo description of the electron identification efficiency introduce a $\pm 5\%$ uncertainty on the final results. The measured jet energies are varied by $\pm 2\%$ at low $p_{T,\text{cal}}^{\text{jet}}$ to $\pm 2.7\%$ at high $p_{T,\text{cal}}^{\text{jet}}$ to account for the uncertainties on

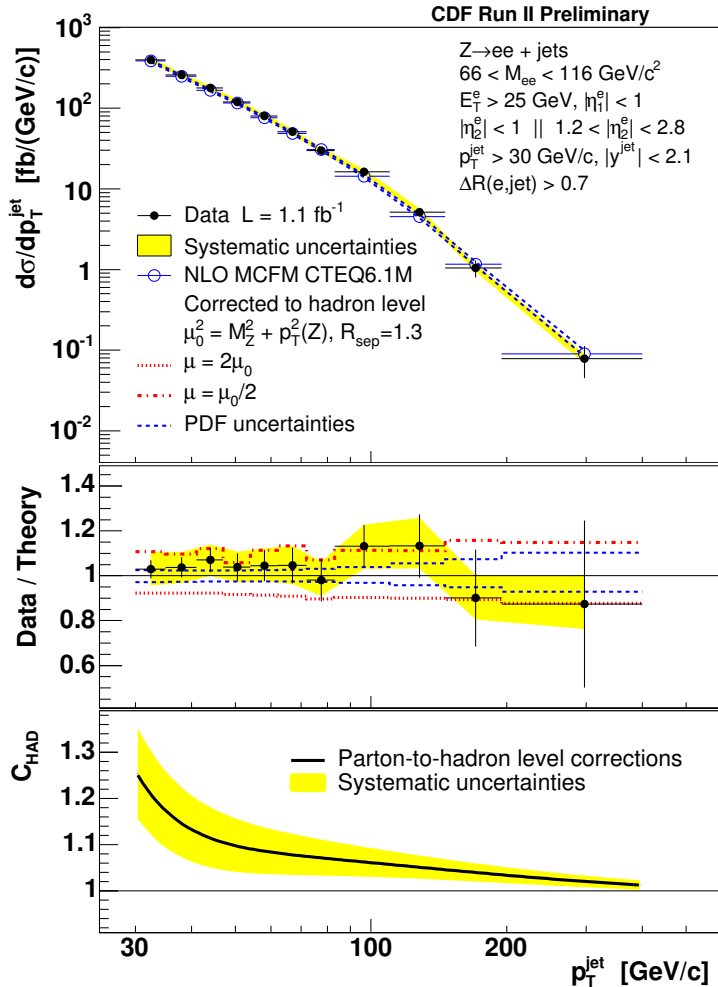


FIG. 2: (top) Measured inclusive jet cross sections (black dots) in $Z(\rightarrow ee) + \text{jet}$ production as a function of p_T^{jet} compared to NLO pQCD predictions (open circles). The shaded bands show the total systematic uncertainty on the measurements. The dashed (dashed-dotted/dotted) lines indicate the PDF (scale) uncertainty on the NLO pQCD predictions. (middle) Ratio data/theory as a function of p_T^{jet} for $N_{\text{jet}} = 1$. (bottom) Parton-to-hadron corrections applied to the pQCD prediction.

the absolute energy scale in the calorimeter [13]; this introduces uncertainties on the final measurements which vary between $\pm 5\%$ at low p_T^{jet} and $\pm 12\%$ at high p_T^{jet} . The uncertainty on the p_T^{jet} dependence of f_e^{jet} introduces a $\pm 15\%$ uncertainty on the QCD-jets and $W + \text{jets}$ background estimation, that translates into a $\pm 1\%$ to $\pm 2\%$ uncertainty on the measured cross sections. A conservative $\pm 30\%$ uncertainty on the normalization of the rest of background contributions, as extracted from Monte Carlo samples, introduces a less than 1% effect on the final results. The unfolding procedure was carried out using unweighted PYTHIA-TUNEA; the effect on the measured cross sections is less than 1%. Finally, the measurements are performed in different periods of Tevatron instantaneous luminosity to account for possible remaining contributions from pile-up events, and no significant effect is found. Positive and negative deviations with respect to the nominal values are added separately in quadrature. A 5.8% uncertainty on the total luminosity is not included in the forthcoming Figures.

VII. RESULTS

Figure 2 shows the measured inclusive jet cross section as a function of p_T^{jet} in $Z(\rightarrow ee) + \geq N_{\text{jet}}$ production with $N_{\text{jet}} = 1$ compared to NLO pQCD predictions. The cross section decreases by more than three orders of magnitude as p_T^{jet} increases from 30 GeV/c up to about 300 GeV/c. The NLO pQCD predictions are computed using the MCFM program [16] with CTEQ6.1M PDFs [17] and the renormalization and factorization scales set to $\mu^2 = M_Z^2 + p_T^2(Z)$.

A variation of μ by a factor two (half) reduces (increases) the theoretical predictions by about $\pm 10\%$ to $\pm 15\%$ as p_T^{jet} increases. The uncertainties on the NLO pQCD predictions due to the uncertainty on the PDFs were computed using the Hessian method [18]. They vary from $\pm 5\%$ at low p_T^{jet} to $\pm 10\%$ at high p_T^{jet} . The theoretical predictions include parton-to-hadron correction factors, $C_{\text{had}}(N_{\text{jet}}, p_T^{\text{jet}})$, that approximately account for non-perturbative contributions from the underlying event and fragmentation into hadrons. C_{had} is estimated, using PYTHIA-TUNE A, as the ratio between the nominal $p_{T,\text{had}}^{\text{jet}}$ distribution and the one obtained by turning off both the interactions between proton and antiproton remnants and the fragmentation in the Monte Carlo samples. The correction decreases as p_T^{jet} increases from about 1.2 at p_T^{jet} of 30 GeV/c to 1.02 at high p_T^{jet} . The uncertainty on C_{had} is about 8% at low p_T^{jet} , as determined using PYTHIA-TUNE DW instead of PYTHIA-TUNE A. Good agreement is observed between the measured cross sections and the theoretical predictions.

Figure 3 shows the total cross section for $Z(\rightarrow ee) + \geq N_{\text{jet}}$ production as a function of the jet multiplicity. The data is compared to LO and NLO pQCD predictions that include parton-to-hadron non-perturbative corrections. For $N_{\text{jet}} = 1$ and $N_{\text{jet}} = 2$, the LO pQCD predictions underestimate the measured cross sections by a factor about 1.3, while good agreement is observed between data and NLO pQCD predictions. For $N_{\text{jet}} = 3$, where no NLO pQCD prediction is available, the data indicates that the measurement can be described by a common LO-to-NLO theoretical factor independent of N_{jet} .

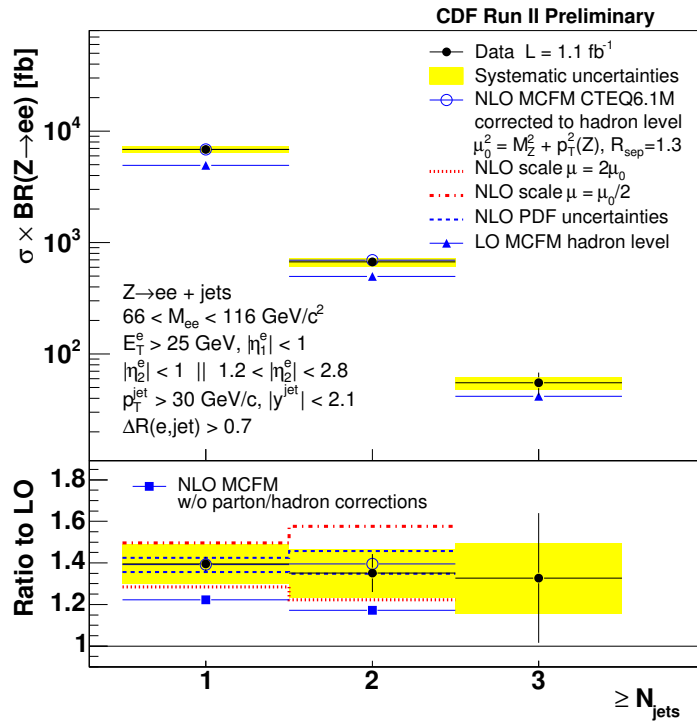


FIG. 3: (top) Measured total cross section for $Z(\rightarrow ee) + \geq N_{\text{jet}}$ production as a function of N_{jet} compared to LO and NLO pQCD predictions. The shaded bands show the total systematic uncertainty on the measurements. The dashed (dashed-dotted/dotted) lines indicate the PDF (scale) uncertainty on the NLO pQCD predictions. (bottom) Ratio of data and NLO to LO pQCD predictions as a function of N_{jet} .

VIII. CONCLUSION

In summary, we have presented results on inclusive $Z(\rightarrow ee) + \geq N_{\text{jet}}$ production in $p\bar{p}$ collisions at $\sqrt{s} = 1.96$ TeV for jets with transverse momentum $p_T^{\text{jet}} > 30$ GeV/c and rapidity in the region $|y^{\text{jet}}| < 2.1$, based on 1.1 fb^{-1} of CDF Run II data. The measured cross sections are in agreement with NLO pQCD predictions.

Acknowledgments

We thank the Fermilab staff and the technical staffs of the participating institutions for their vital contributions. This work was supported by the U.S. Department of Energy and National Science Foundation; the Italian Istituto

Nazionale di Fisica Nucleare; the Ministry of Education, Culture, Sports, Science and Technology of Japan; the Natural Sciences and Engineering Research Council of Canada; the National Science Council of the Republic of China; the Swiss National Science Foundation; the A.P. Sloan Foundation; the Bundesministerium für Bildung und Forschung, Germany; the Korean Science and Engineering Foundation and the Korean Research Foundation; the Particle Physics and Astronomy Research Council and the Royal Society, UK; the Institut National de Physique Nucléaire et Physique des Particules/CNRS; the Russian Foundation for Basic Research; the Comisión Interministerial de Ciencia y Tecnología, Spain; the European Community's Human Potential Programme under contract HPRN-CT-2002-00292; and the Academy of Finland.

- [1] D.J. Gross and F. Wilczek, Phys. Rev. D **8**, 3633 (1973).
- [2] T. Affolder *et al.* (CDF Collaboration), Phys. Rev. D **63**, 072003 (2001).
F. Abe *et al.* (CDF Collaboration), Phys. Rev. Lett. **77**, 448 (1996).
V. M. Abazov *et al.* (D0 Collaboration), arXiv:hep-ex/0608052.
- [3] The hadron level in the Monte Carlo generators is defined using all final-state particles with lifetime above 10^{-11} s.
- [4] R. Brun *et al.*, Tech. Rep. CERN-DD/EE/84-1, 1987.
- [5] G. Grindhammer, M. Rudowicz and S. Peters, Nucl. Instrum. Meth. A **290**, 469 (1990).
- [6] T. Sjöstrand *et al.*, Comp. Phys. Comm. **135**, 238 (2001).
- [7] H.L. Lai *et al.*, Eur. Phys. J. C **12**, 375 (2000).
- [8] T. Affolder *et al.* (CDF Collaboration), Phys. Rev. D **65**, 092002 (2002).
- [9] R. Field, FERMILAB-CONF-06-408-E, FNAL (2005).
- [10] G. C. Blazey, *et al.*, arXiv:hep-ex/0005012 (2000).
- [11] Here “electron” is used to denote electrons and positrons.
- [12] S.R. Hahn *et al.*, Nucl. Instrum. Meth. A **267**, 351 (1988).
- [13] A. Bhatti *et al.*, Nucl. Instrum. Meth. A **566**, 375 (2006).
- [14] D. Acosta *et al.* (CDF Collaboration), Phys. Rev. Lett. **B94**, 091803 (2005).
- [15] Oriol Saltó, Ph.D. Thesis, Universitat Autònoma de Barcelona, in preparation.
- [16] J. Campbell, R.K. Ellis, Phys. Rev. D **65**, 113007 (2002).
- [17] J. Pumplin *et al.*, JHEP **0207**, 012 (2002).
- [18] J. Pumplin *et al.*, Phys. Rev. D **65**, 014013 (2002).